DTU Library

Plate microstructures with extreme stiffness for arbitrary multi-loadings

Wang, Yiqiang; Groen, Jeroen P.; Sigmund, Ole

Published in:
Computer Methods in Applied Mechanics and Engineering

Link to article, DOI:
10.1016/j.cma.2021.113778

Publication date:
2021

Document Version
Peer reviewed version

Plate microstructures with extreme stiffness for arbitrary multi-loadings

Yiqiang Wang[a,b,*], Jeroen P. Groen[b], Ole Sigmund[b]

[a] *State Key Laboratory of Structural Analysis for Industrial Equipment, Dalian University of Technology, Dalian 116024, China*

[b] *Department of Mechanical Engineering, Solid Mechanics, Technical University of Denmark, Building 404, 2800 Kongens Lyngby, Denmark*

Abstract

Mechanical metamaterials that achieve ultimate anisotropic stiffness are highly desired in engineering practice. Particularly, the plate microstructures (PM) that are comprised of 6 sets of flat plates have been proved to attain any extreme stiffness in theory. In this paper, we solve two remaining issues for design of optimal PMs. On one hand, we investigate the stiffness optimality of three PMs that involve fewer than 6 freely-oriented plate sets subjected to any prescribed multi-loadings, which are typically quasiperiodic. Because they have simpler geometries with fewer plate sets, they are preferred in practical applications. On the other hand, we identify two optimal periodic plate lattice structures which are comprised of 7 plate sets, and demonstrate that they are able to attain near-optimal stiffness (over 97% and 99% of the extreme stiffness in theory) for any multi-loadings in the low volume fraction limit. In order to ensure a sufficiently large loading space for verification of the stiffness optimality of these PMs, tens of thousands of random multi-loadings are first used and further the worst multi-loading that yields the highest stiffness deficiency is systematically identified for each PM. The numerical results not only illustrate the stiffness optimality of these PMs, but also provide suggestions on selection of the simplest PMs with the fewest plate sets in applications.

Keywords: mechanical metamaterial, plate microstructures, extreme stiffness, anisotropic stiffness, multiple loadings

1. Introduction

Mechanical metamaterials are artificial materials whose effective properties are determined by their microstructures [1–3]. They provide either superior mechanical properties that are beyond naturally existing materials [4–12], or unusual functionalities [13–16]. Rapid advance of manufacturing techniques provides fabrication capabilities of mechanical metamaterials with complex geometries, whose feature sizes can be down to tens of nanometers [17–19]. Hence, mechanical metamaterials with extreme properties are becoming realizable and attractive.

Long-term efforts have been devoted to design of symmetric elastic microstructures with ultimate stiffness defined by the Hashin–Shtrikman bounds [20, 21]. Several optimal cubic materials have been identified, such as three elementary cubic structures (i. e. simple cubic, body-centered cubic

*Corresponding author: wangyq@dlut.edu.cn

and face-centered cubic) [22], composite sphere assemblages [20], Vigdergauz microstructures [23, 24], and minimal-surface microstructures (like P-surface) [25]. These can attain the extreme bulk modulus, but cannot attain optimal shear modulus at the same time. A class of lattice structures was formed by synthesizing two or more elementary cubic structures to attain optimal isotropic stiffness in the sense that they simultaneously attain the maximum bulk, shear and Young's moduli [26–30]. Recently, the authors identified a new family of quasi-periodic microstructures [31] which use n-fold rotational geometric symmetries to achieve optimal isotropic stiffness. In the case of 6-fold symmetry, the microstructures become periodic and can be represented by parallelepiped unit cells. It is worth noting that the extreme stiffness in theory can be exactly attained only by the plate microstructures (PMs), while the truss microstructures suffer from essential stiffness deficiency. In the case of isotropic stiffness, the truss microstructures reach as little as one third of the extreme stiffness provided by the PMs in the low volume fraction limit [21, 32].

Anisotropic stiffness-optimal microstructures are more efficient for bearing multi-loadings, however they are difficult to identify. In single loading cases, orthotropic microstructures involving 3 sets of orthogonal members are optimal when aligning the members with principal stress or strain directions [33]. Several groups proposed rank-n microstructures to attain the extreme stiffness for arbitrary multi-loadings [34–36]. These rank-n microstructures are built by a sequential layering of flat plates at n separated length scales, where no more than $n = 3$ and $n = 6$ are needed for 2D and 3D problems, respectively. Remark that in the low volume fraction limit, the rank-n microstructures possess the same properties as their single-scale counterparts [37]. Therefore, in that case, the single-scale counterparts with 6 sets of flat plates can attain any extreme stiffness in theory. Another class of optimal microstructures combines solid domains with rank members [38]. They were first used to achieve the maximum bulk modulus and almost minimum shear modulus, but their construction can be extended to any anisotropic case. Recently, four categories of optimal truss microstructures were identified to attain near-optimal stiffness for arbitrary multi-loadings [39].

Despite above efforts, two issues are remained. One issue is that compared to the optimal PMs with 6 plate sets, the PMs that involve fewer plate sets are preferable in engineering practice [40]; however, their stiffness optimality subjected to any multi-loadings has yet to be examined, and therefore no guideline can be made on how to select the simplest PMs with the fewest plate sets in applications. The other issue is that since the optimal PMs with free plate sets are typically quasiperiodic, in the sense that each plate set reappears infinitely but the PMs can never be described in a periodic form, they may have limitations in applications. Only in the condition that the plate sets meet periodic connections, the PMs become periodic, which is usually referred to as plate lattice structures (PLSs). To the authors' best knowledge, the optimal PLSs that can attain any extreme stiffness has yet to be identified.

In this paper, we intend to address these two issues. On one hand, we investigate the stiffness optimality of three PMs which involve 3 to 5 plate sets that can be freely oriented. On the other hand, we identify two optimal PLSs which can attain the extreme stiffness for any multi-loadings. The two PLSs have 7 plate sets, whose plate connections originate from two optimal isotropic PLSs, which are a combined PLS involving simple and body-centered cubic structures [26, 27] and a PLS possessing 6-fold symmetry [31]. For prescribed multi-loadings, the plate orientations and thicknesses of the considered PMs are optimized to achieve the maximum stiffness. The optimization problems are solved in the low volume fraction limit, in which the intersecting regions of different plate sets play marginal roles on the effective stiffness. We verify stiffness optimality of these PMs first by tens of thousands of random multi-loadings, which are generated via various strategies, and further by identification of the worst case multi-loadings, which result in the highest stiffness deficiency. Numerical results demonstrate that, for arbitrary multi-loadings, the three PMs with free plate sets achieve over 83.5%, 90% and 95% of the extreme stiffness, and the two PLSs attain near-optimal stiffness with over 97% and 99% of the extreme stiffness. With the obtained optimal plate orientations, PMs for moderate volume fractions can be directly constructed by proportionally increasing the plate thicknesses. In that case, the plate intersections would cause local stress concentrations, but according to the numerical studies from [26, 27, 31], the PMs suffer from stiffness deficiency of only a few percent for volume fractions up to 50%.

The paper is organized as follows. In section 2, we illustrate configurations of our considered PMs as well as the parameters to describe their geometries. In section 3, optimization problems are set up to obtain the extreme stiffness in theory by using the rank-6 microstructures. In section 4, we study stiffness optimality of our considered PMs with respect to thousands of prescribed random multi-loadings, and in section 5, the worst multi-loadings that obtain the highest stiffness deficiency for each PM are systematically identified. A conclusion is made in the final section.

2. Geometries of considered PMs

The considered microstructures are synthesized by n sets of continuously flat plates, and each set involves infinite equidistant and parallel plates. Typically, these plate sets can be freely oriented, and thus the PMs are typically quasiperiodic. In the following, the PMs with n free plate sets are denoted by PM-n. Different from the rank-n microstructures that involve multi-scale members (Fig. 1a), PM-n are formed by n plate sets at the same single scale (Fig. 1b). The volume fraction of solid domains in the microstructure is denoted by ρ. Remark that in the low volume fraction limit, i. e. $\rho \to 0$, the rank-n microstructures and PM-n that have the same plate orientations and thicknesses possess identical effective stiffness [37]. Hence, PM-6 is able to achieve the optimal stiffness for arbitrary multi-loadings in case of $\rho \to 0$. To this end, we are more interested in stiffness optimality of PM-3, PM-4 and PM-5 for any applied multi-loadings, as they have simpler geometries with fewer plate sets. Here, PM-3 has the smallest number of plate sets necessary to achieve optimal stiffness for any single-loadings.

In addition, we investigate stiffness optimality of two PLSs involving $n = 7$ plate sets. Compared to three above PM-n with free plate sets, the two PLS7s have periodic plate connections, and thus they can be represented by periodic unit cells (Fig. 1c). Their designs arise from two optimal isotropic PLSs. One PLS7 is synthesized by 3 sets of simple cubic plates and 4 sets of body-centered cubic plates [26, 27], denoted by PLS7-SB. The other PLS7 is shaped in a diamond-like prism that is formed by 1 horizontal plate set and 6 inclined plate sets that meet the 6-fold symmetry [31], denoted by PLS7-6Fold. Although there are many other optimal isotropic microstructures [27, 31], these two PLS7s most probably involve the least number of plate sets among all the PLSs that can achieve the near-optimal isotropic stiffness. Because optimal isotropic stiffness is very special as the elastic stiffness tensor meets infinite symmetries, we expect that any other extreme anisotropic stiffness with lower order of material symmetries could be obtained by modifications of these two PLS7s.

In order to describe geometries of the three PM-n and two PLS7s, different representation methods are applied (Fig. 1d). The three PM-n are represented by geometric parameters of the plate sets. In each PM-n, $\tilde{t}_i$ indicates the proportion of solid domains of the ith plate set among all the plate sets, meeting $\sum \tilde{t}_i = 1$. In the low volume fraction limit $\rho \to 0$, the volume fraction of solid domains of the ith plate set in the microstructure is obtained by $\rho\tilde{t}_i$. It is further related to the plate thickness t_i and the distance between two neighboring plates d_i as $\rho\tilde{t}_i = t_i/d_i$. Furthermore, the plate orientations are characterized by normal directions $\boldsymbol{n}_i$, which are stated in terms of two angles by (Fig. 1d left)

$$\boldsymbol{n}_i = \{\cos\theta_{2i-1}\cos\theta_{2i},\ \cos\theta_{2i-1}\sin\theta_{2i},\ \sin\theta_{2i-1}\}^{\mathrm{T}}, \quad (i = 1, 2, ..., n) \tag{1}$$

For the two PLS7s, their unit cells can be flexibly transformed to parallelepipeds to achieve the maximum stiffness for prescribed multi-loadings. Two sets of parameters are used to describe shapes of the unit cells (Fig. 1d right). One set is used to represent three periodic directions, in which the ith periodic direction is characterized by two angles Θ_{2i-1} and Θ_{2i} in the same way as Eq. (1). For three periodic directions, totally six angle parameters are employed. The other set of parameters determines periodic distances. Since no length scale effect is considered for evaluating the effective properties, two variables s_1 and s_2 are used to denote the relative periodic distances along two periodic directions with respect to the third one. During transformation, the plate connections are retained. In this sense, the normal direction of each plate set in one PLS7 can be uniquely determined in terms of Θ_i and s_j.

Several remarks are made. Firstly, the two PLS7s have distinct plate connections in the sense that with any transformation, one PLS7 cannot be reproduced by the other one. Hence, they might cover different stiffness spaces and have different stiffness optimality subjected to various multi-loadings. Secondly, the unit cells can be transformed by any rotations and elongations by varying Θ_i and s_j, but never by distortions (twisting the cells). Thirdly, in case of $\rho \to 0$, adjusting spatial positions of the plate sets but retaining $\tilde{t}_i$ would not change the effective properties. In this sense, PM-3 and PM-4 can always be represented by periodic parallelepiped unit cells. However, PM-5 may never be periodic. Finally, individual plate sets can be removed in the microstructures, by setting $\tilde{t}_i = 0$. This implies that the two PLS7s and PM-5 can reproduce any geometries from PM-4 and PM-3, and thus they cover larger property spaces. However, because of the implicit restriction applied on geometries of the two PLS7s, they have different design spaces from PM-5. Consequently, they might obtain different stiffness optimality with respect to various multi-loadings.

3. Extreme stiffness by rank-6 microstructure

In this study, because our concerned PMs are anisotropic, we use the stress energy to indicate their stiffness optimality when subjected to prescribed multi-loadings. For stress loadings, the optimal microstructure that has the highest stiffness is found by solving an optimization problem, which is stated by

$$\begin{aligned} \underset{\boldsymbol{\chi}}{\text{Minimize}} \quad & J = \sum_{r=1}^{N_\sigma} w_r \boldsymbol{\sigma}^{(r)} : \boldsymbol{C}^{\mathrm{H}}(\boldsymbol{\chi}, \rho) : \boldsymbol{\sigma}^{(r)} \\ \text{Subject to} \quad & \sum_{k=1}^{6} \tilde{t}_k = 1 \\ & \underline{\chi} \le \chi_i \le \overline{\chi} \end{aligned} \tag{2}$$

where J is the weighted stress energy subjected to the prescribed multi-loading that involves N_σ stress cases, in which each stress case is denoted by $\boldsymbol{\sigma}^{(r)}$, w_r is the weighting factor which is normalized for $\sum w_r = 1$, $\boldsymbol{\chi}$ indicates the design variable vector including various sets of geometric

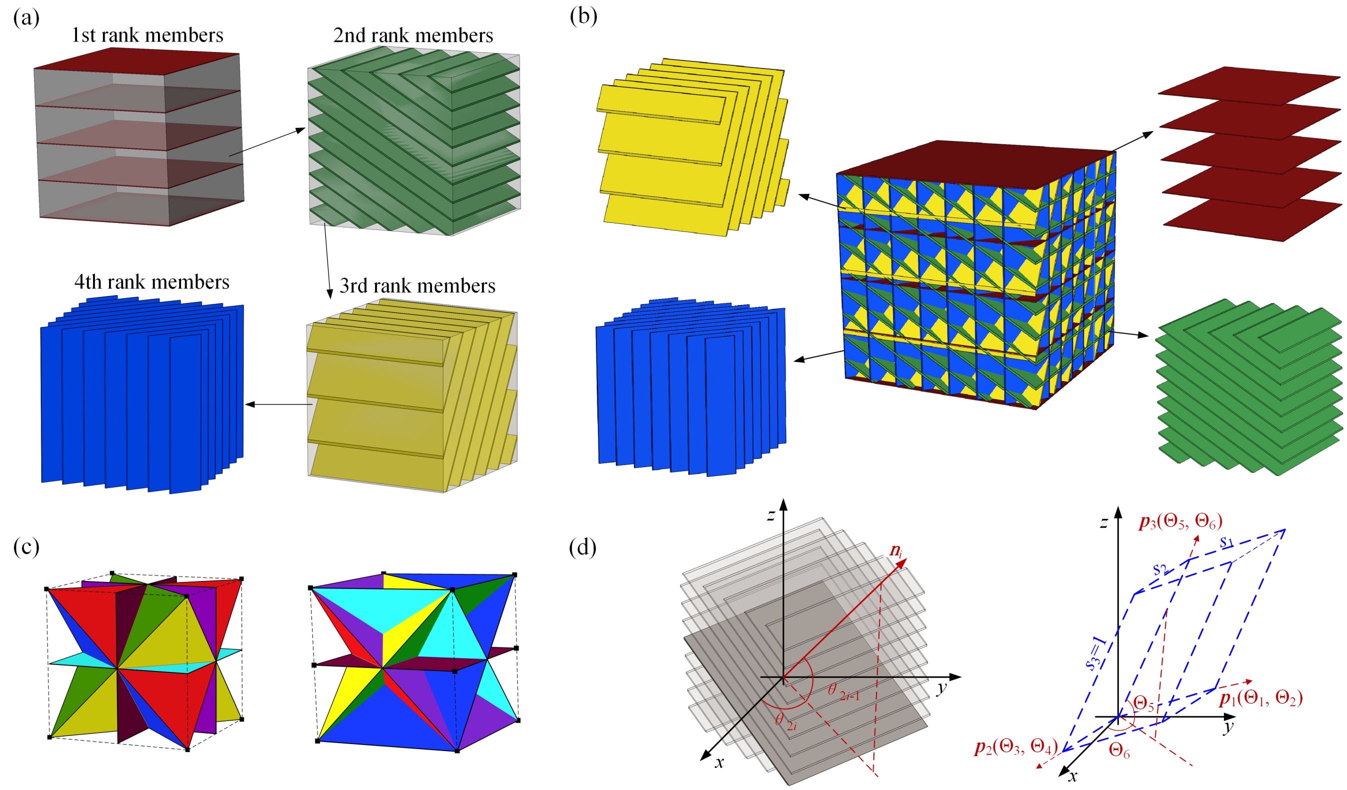

Figure 1: Configurations of the considered PMs. (a) Rank-n microstructures including multiscale members, where grey regions indicate uniform materials in the lower scale level; (b) Our considered PMs formed by sets of continuously flat plates at the single scale, where the number of plate sets can be varied to have PM-3, PM-4 and PM-5; (c) Unit cells for two PLS7s that have distinct plate connections; (d) Parameter descriptions for PMs with free plate sets (left) and PLSs with unit cells (right). Different colors are used to indicate the plates from various sets.

parameters for different microstructures, with lower and upper bounds denoted by $\underline{\chi}$ and $\overline{\chi}$, respectively, and $\boldsymbol{C}^{\mathrm{H}}$ is the compliance tensor, which is related to the geometric variables $\boldsymbol{\chi}$ as well as the relative volume fraction ρ.

In order to obtain the extreme stiffness in theory, we solve the optimization problem by the rank-6 microstructures. In that case, the optimal proportional thickness and orientation of each rank member are determined, and the design variable vector includes $\boldsymbol{\chi} = \{\theta_i, \tilde{t}_k\}$, for $i = 1, 2, ..., 12$ and $k = 1, 2, ..., 6$ and in the condition of $-2\pi \leq \theta_i \leq 2\pi$ and $0 \leq \tilde{t}_k \leq 1$. The compliance tensor of the rank-6 microstructures can be analytically calculated based on $\tilde{t}_k$, θ_i and ρ [41–43], where ρ is manually prescribed. The optimal geometries that attain one extreme stiffness could be non-unique. In order to identify the optimal microstructures involving the least number of rank members, one way is to incorporate a penalization term with 2-norm of $\tilde{t}_k$ into the objective function [37, 39]. Note that the multiscale members ensure ideal force transfer between various plate sets, hence solving this optimization yields the theoretical bounds for any $0 < \rho \leq 1$.

This optimization problem includes only 18 geometric variables, and therefore it can be efficiently solved by gradient-based optimization algorithms. The gradient of the stress energy reads

$$\frac{\partial J}{\partial \chi} = \sum_{r=1}^{N_\sigma} w_r \boldsymbol{\sigma}^{(r)} : \frac{\partial \boldsymbol{C}^{\mathrm{H}}}{\partial \chi} : \boldsymbol{\sigma}^{(r)}, \quad \text{such that} \quad \frac{\partial \boldsymbol{C}^{\mathrm{H}}}{\partial \chi} = -\boldsymbol{C}^{\mathrm{H}} : \frac{\partial \boldsymbol{D}^{\mathrm{H}}}{\partial \chi} : \boldsymbol{C}^{\mathrm{H}} \tag{3}$$

where $\partial \boldsymbol{D}^{\mathrm{H}}/\partial \chi$ can be analytically calculated for the rank-6 microstructures. Derivatives of the linear constraints are one with respect to $\tilde{t}_k$ and zero with respect to the other variables.

4. Stiffness optimality for prescribed multi-loadings

4.1. Optimization formulations for prescribed multi-loadings

The maximum stiffness for the prescribed multi-loadings by the considered PMs is obtained by solving the same optimization problem as Eq. (2). Different from the rank-6 microstructures, we here focus on optimizations in the low volume fraction limit $\rho \to 0$. In that case, stiffness contribution from the ith plate set is linearly proportional to its proportional thickness $\tilde{t}_i$. Hence, the stiffness tensor $\boldsymbol{D}^{\mathrm{H}}$ can be calculated by a superposition (add-up) law, which linearly sums up the transformed stiffnesses from each individual plate set by,

$$\boldsymbol{D}^{\mathrm{H}} = \sum_{i=1}^{N} \rho \tilde{t}_i \boldsymbol{D}_i = \sum_{i=1}^{N} \rho \tilde{t}_i \boldsymbol{T}_i : \boldsymbol{D}_{\mathrm{s}} : \boldsymbol{T}_i \tag{4}$$

where $\boldsymbol{D}_{\mathrm{s}}$ indicates the stiffness tensor for a single solid plate set with a unit thickness, $\boldsymbol{D}_i$ is the corresponding transformed stiffness tensor, and $\boldsymbol{T}_i = \boldsymbol{T}(\boldsymbol{n}_i)$ is the transformation tensor for the ith plate set, which relates to the orientations of the plate sets and its formulation can be found in the textbook, e. g. [44].

This superposition model is able to exactly estimate the effective stiffness in case of $\rho \to 0$. In moderate volume fractions, this model typically causes prediction errors due to the effects of intersecting regions, and the error gets quadratically smaller with lower volume fractions. For instance, for $\rho = 10\%$ and 5%, this model underestimates the effective Young's modulus of the optimal isotropic 6-fold PLS by about 4% and 1% compared to the result from the numerical homogenization method [31]. The superposition law works effectively for any microstructures that have continuous members, where the resulting microstructures can be either periodic or quasiperiodic and they can be formed by either flat plates or straight trusses [21, 31, 37]. Note that the calculated $\boldsymbol{D}^{\mathrm{H}}$ does not rely on the applied strain or stress loadings, since it is an essential property of the PM. By using this explicit model, the derivative of $\boldsymbol{D}^{\mathrm{H}}$ with respect to the geometric parameters can be directly obtained.

In the optimization, the compliance tensor $\boldsymbol{C}^{\mathrm{H}}$ of each PM is calculated by the inverse of $\boldsymbol{D}^{\mathrm{H}}$. In order to determine the optimal plate orientations and proportional thicknesses, for the three PM-n, the design variable vector includes $\boldsymbol{\chi} = \{\theta_i,\, \tilde{t}_k\}$, for $i = 1, 2, ..., 2n$ and $k = 1, 2, ..., n$. For the two PLS7s, the cell shapes are optimized to vary the plate orientations, and the design variable vector includes $\boldsymbol{\chi} = \{\Theta_i,\, s_j,\, \tilde{t}_k\}$, for $i = 1, 2, ..., 6$, $j = 1, 2$ and $k = 1, 2, ..., n$, respectively. The lower bound for s_j is set to be $\underline{s} = 0.1$, which prevents excessive cell distortions. In the optimized results, any plate set(s) can be removed by $\tilde{t}_k = 0$.

The optimization problems include at most 15 design variables (for PM-5 and the two PLS7s). The gradient of the stress energy has the same form as Eq. (3), and the derivative of the linear constraints are one with respect to $\tilde{t}_k$ and zero with respect to the other variables. The optimality conditions are

$$
\begin{aligned}
&\frac{\partial J}{\partial \tilde{t}_p} = \sum_{r=1}^{N_\sigma} \rho w_r (\boldsymbol{\sigma}^{(r)} : \boldsymbol{C}^{\mathrm{H}}) : \boldsymbol{D}_p : (\boldsymbol{C}^{\mathrm{H}} : \boldsymbol{\sigma}^{(r)}) = \lambda, \quad (p = 1, 2, ..., n) \\
&\frac{\partial J}{\partial \theta_i} = \frac{\partial J}{\partial s_j} = \frac{\partial J}{\partial \Theta_q} = 0, \quad (i = 1, 2, ..., 2n; j = 1, 2; q = 1, 2, ..., 12)
\end{aligned}
\tag{5}
$$

where λ is the Lagrange multiplier applied on the linear constraints. The first condition indicates a uniform strain energy density distribution, which implies that all the plates are equally used to bear the multi-loading, and the second conditions indicate optimal plate orientations.

4.2. Generation of random multi-loadings

Stiffness optimality of the three PM-n and the two PLS7s are first verified for random multi-loadings. Because each $\boldsymbol{\sigma}^{(r)}$ includes three normal and three shear stress components, at most 6 stress cases are linearly independent, and any extra stress case is linearly dependent on them. Hence, we consider multi-loadings with $2 \leq N_\sigma \leq 6$ independent stress cases in this study. Furthermore, in order to normalize the generated stress cases, we define a mathematical fourth-order tensor to represent a weighting summation of all the stress cases by

$$
\boldsymbol{\Gamma} = \Gamma_{ijkl} = \sum\nolimits_{r=1}^{N_\sigma} w_r \sigma_{ij}^{(r)} \sigma_{kl}^{(r)} \tag{6}
$$

where repeated subscripts indicate summation from 1 to 3. In this way, the stress energy can also be stated by $J = \Gamma_{ijkl} C_{ijkl}^{\mathrm{H}}$.

Three strategies are employed to generate random multi-loadings. In strategy I, all the 6 terms in each stress case of one multi-loading are randomly generated within the internal [-1, 1] by

$$
\sigma_{ij}^{(r)} = 2\Phi - 1, (ij = 11, 22, 33, 23, 13, 12; r = 1, 2, ..., N_\sigma) \tag{7}
$$

where Φ indicates the embedded function *rand* in Matlab, which generates uniformly-distributed random numbers.

In strategy II, for each stress case in one multi-loading scenario, 3 random principal stresses are first generated by Eq. (7), which are denoted by $\tilde{\boldsymbol{\sigma}}^{(r)}$. Then, $\tilde{\boldsymbol{\sigma}}^{(r)}$ is rotated in a sequential order along x, y and z axis, in which the rotation angles are randomly generated within $[-\pi, \pi]$. The corresponding rotation tensor is denoted by $R_{ij} = R_{ip}^{x} R_{pq}^{y} R_{qj}^{z}$, where the superscripts indicate the rotation axis. The final stress case is obtained by

$$
\sigma_{ij}^{(r)} = R_{ip} \tilde{\sigma}_{pq}^{(r)} R_{qj}, \quad (i, j = 1, 2, 3; r = 1, 2, ..., N_\sigma) \tag{8}
$$

In both strategies, the weighting factors are also randomly generated within [0, 1]. Moreover, both the stresses and weighting factors are normalized by $\boldsymbol{\sigma}^{(r)}/\|\boldsymbol{\Gamma}\|_{\mathrm{F}}$ and $w_r/\sum w_r$, respectively, in which $\|\square\|_{\mathrm{F}}$ is the Frobenius norm. The regularized stresses will be applied in the optimizations. For each N_σ, 500 random multi-loadings are generated by using each strategy.

Furthermore, strategy III is made to generate random multi-loadings around the isotropic multi-loading case, which refers to the multi-loading that results in optimal isotropic stiffness. Essentially, $\boldsymbol{\Gamma}$ formed by the isotropic multi-loading through Eq. (6) meets infinite symmetries. Here, we employ one isotropic multi-loading that involves 6 uniaxial stress cases in a 5-fold rotational symmetric way, which is stated by

$$\boldsymbol{\sigma}_{\text{iso}}^{(1)} = [0,0,1,0,0,0]^{\text{T}}, \quad \boldsymbol{\sigma}_{\text{iso}}^{(r)} = \boldsymbol{\sigma}_0^{(r)} \otimes \boldsymbol{\sigma}_0^{(r)}, \quad (r = 2,3,...,6) \tag{9}$$

where $\boldsymbol{\sigma}_0^{(r)} = [\cos\alpha\cos\beta r, \cos\alpha\sin\beta r, \sin\alpha]^{\text{T}}$ with $\sin^2\alpha = 4/5$ and $\beta = 2\pi/5$. The weighting factors are $w_r = 1/6$. Random perturbations are made to both stress terms in each stress case and weighting factors to create random multi-loadings

$$\sigma_{ij}^{(r)} = (1 + mf_r)(\sigma_{\text{iso}}^{(r)})_{ij}, \quad w_r = (1 + mg_r)w_r, \quad (i,j = 1,2,3; r = 1,2,...,N_\sigma) \tag{10}$$

where $f_r, g_r = 2\Phi - 1$ and m is a factor to control the perturbation magnitude, which is evaluated by $m = \pm 5\%, 10\%, 15\%, 20\%, 25\%$. For each m value, 50 random values are generated, and totally 500 perturbations are created. Furthermore, other random multi-loadings with $N_\sigma < 6$ are also generated by removing specific number of stress cases.

4.3. Implementation

The above optimization problems are solved by using the interior-point method that is embedded in optimizer *fmincon* in Matlab. The procedure is terminated if either the maximum difference of both objective functions and design variables between two subsequent iterations are smaller than 10^{-10} or maximum 1000 iterations are reached. For each multi-loading, 200 random initial guesses are used for each PM testing, and the minimal stress energy among the 200 optimized solutions is referred to the maximum stiffness that this PM can achieve. In this way, totally $3 \times 5 \times 500 \times 200 \times 6 = 9 \times 10^6$ optimization problems are solved. In all testing, Young's modulus and Poisson's ratio of the solid constituent are $E_{\text{s}} = 1$ and $\nu_0 = 1/3$, respectively. The maximum value for the relative edge length is $\bar{s} = 5$.

We use an energy ratio R to indicate stiffness optimality (or deficiency) of each PM, which is defined by

$$R = \frac{J_{\text{Rank6}}^{\text{opt}} \times \rho_{\text{Rank6}}}{J_{\text{PM}}^{\text{opt}} \times \rho_{\text{PM}}} \times 100\% \tag{11}$$

where superscript 'opt' indicates the optimal energy when optimizations converge. The optimized microstructures attain the extreme stiffness if $R = 1$, and suffer from higher stiffness deficiency as R gets smaller. In the equation, both the extreme energy by the rank-6 microstructures and the optimal energy by the PMs are normalized by their volume fractions. There, we use $\rho_{\text{Rank6}} = 10^{-6}$ for obtaining the extreme stiffness, where a smaller value may cause numerical issues. In the optimization for the PMs, we simply take $\rho_{\text{PM}} = 1$, as ρ in Eq. (4) is merely a scaling parameter.

We also measure the anisotropy level of the optimal microstructures by using an index

$$A = \frac{M}{M_{\text{iso}}}, \quad \text{with} \quad M = \frac{\sum_{i=1}^{6} e_i}{\sqrt{\sum_{i=1}^{6} e_i^2}} \tag{12}$$

where e_i is the ith eigenvalue of the stiffness tensor of the optimal microstructures, and M_{iso} is for the optimal isotropy, which is also the maximum value of M. The maximum value $A = 1$ indicates that the extreme stiffness is isotropic, and it indicates higher order of anisotropy as A gets smaller. The minimum value is $A = \sqrt{8/15} \approx 0.73$ (for $\nu_0 = 1/3$), which arises when the PM includes a single plate set. To ensure rotational invariance of the eigenvalues, the stiffness tensor is represented in its second-rank tensor notation [45]. In each multi-loading, we will use the anisotropy level of the optimal rank-6 microstructures for comparisons of stiffness optimality of various PMs, which is denoted by $A_{\text{rank-6}}$. Moreover, the anisotropy level of the optimal PM is indicated by a corresponding subscript, such as $A_{\text{PM-3}}$ for PM-3.

4.4. Results

The obtained energy ratios for various N_σ are presented in Fig. 2. The stiffness optimality of each PM is measured by the minimal R value among the solutions for 500 random multi-loadings in each stress generation strategy, which are given in Table 1. It is seen that increasing N_σ makes the effective stiffness of the optimal rank-6 microstructures more isotropic. The results for $N_\sigma = 2$ (red dots) have the highest anisotropy with $0.77 < A_{\text{rank-6}} < 0.87$, while the results for $N_\sigma = 6$ (blue samples) are closer to isotropy with $0.87 < A_{\text{rank-6}} < 0.97$. The results for strategies I and II (circular and square samples) do not reach pure isotropy. For comparisons, small perturbations on the isotropic multi-loading in strategy III obtains optimal stiffness around pure isotropy (triangular samples), with $0.96 < A_{\text{rank-6}} \leq 1.00$. On the other end, no results are found to be within $\sqrt{8/15} < A_{\text{rank-6}} < 0.77$. This part might correspond to the optimal results for single loadings, in which case, the microstructures with simple geometries, like the ones involving 3 plate sets, could achieve the extreme stiffness.

From Fig. 2, it is seen that PM-3, PM-4 and PM-5 have similar shapes of stiffness optimality, in which their stiffness optimalities decay as N_σ increases. Particularly, this tendency is more obvious for the multi-loadings in strategy III than the cases in strategies I and II when $A_{\text{rank-6}}$ approaches isotropy. Therein, PM-3 is able to achieve $R > 98\%$ of the extreme stiffness for $N_\sigma = 2$ and $R > 86\%$ for $N_\sigma \geq 3$. For comparisons, PM-4 and PM-5 gain improvement on stiffness optimality by incorporating more plate sets. In Table 1, PM-3 shows a slightly higher minimal R value for $N_\sigma = 4$ than $N_\sigma = 3$. This may be because the generated random multi-loadings for $N_\sigma = 4$ do not cover the worst case multi-loading for $N_\sigma = 3$. The results subjected to the worst multi-loadings show a monotonous decrease of R by increasing N_σ (see section 5).

When the isotropic multi-loading is applied, PM-3, PM-4 and PM-5 all suffer from the highest stiffness deficiency with $R = 86.82\%$, $R = 92.78\%$ and $R = 96.33\%$, respectively. In the corresponding geometry for PM-3, 3 plate sets with an equal $\tilde{t} = 1/3$ form the side faces of a regular triangular prism, where the relative angle between each two plate sets is $2\pi/3$. This geometry has a 3-fold rotational symmetry (see Fig. 3(a)). The optimized PM-4 is described as a full regular triangular prism, where 3 plate sets form the side faces and the other plate set forms the base faces (see Fig. 3(b)), with a relationship of $\tilde{t}_{\text{side}}/\tilde{t}_{\text{base}} \approx 0.73$. In the optimized PM-5, all the plate sets are oriented in a 5-rotational symmetry (see Fig. 3(c)), where they have an equal $\tilde{t} = 1/5$ and the relative angle between each two neighboring plate sets is about 69-degree. These geometries might have shown the highest symmetric order that each PM-n can achieve. Particularly, by adding one extra plate set to the optimized PM-5 and adjusting $\tilde{t}$ and the relative angle between each two neighboring plate sets, a 5-fold microstructure that achieves optimal isotropy is produced [31]. Note that the obtained stiffness of these optimized PM-n are anisotropic, with $A_{\text{PM-3}} = 0.91$, $A_{\text{PM-4}} = 0.97$ and $A_{\text{PM-5}} = 0.99$.

The two PLS7s are superior to the three PM-n. In all testing, PLS7-SB and PLS7-6Fold obtain $R > 99.20\%$ and $R > 99.70\%$ of the extreme stiffness, respectively. The worst cases for PLS7-SB and PLS7-6Fold are found around $A_{\text{rank-6}} = 0.97$ and $A_{\text{rank-6}} = 0.95$, respectively, when they are subjected to random multi-loadings from strategy I with $N_\sigma = 6$. The corresponding geometries for PLS7-SB and PLS7-6Fold include 6 and 5 plate sets, respectively. However, they are difficult to describe because of their non-uniform $\tilde{t}$ and non-regular plate orientations. Compared to the rank-6 microstructures, the two PLS7s are periodic and have unique plate connections, and therefore, they might be easier to be recognized and manufactured in practical applications.

Table 1 Minimum R for each PM among the 500 solutions by using each stress generation strategy (abbreviation by ST). Underlines are marked on the smallest values among three strategies for each N_σ.

	ST \ N_σ	2	3	4	5	6
PM-3	I	<u>98.26</u>	<u>93.17</u>	93.21	<u>92.28</u>	91.56
	II	98.87	95.01	<u>91.55</u>	93.02	91.93
	III	99.41	96.24	96.27	93.23	<u>86.82</u>
PM-4	I	<u>99.99</u>	<u>99.83</u>	<u>98.51</u>	<u>98.38</u>	98.38
	II	99.99	99.98	99.50	98.53	98.55
	III	99.99	99.99	99.72	98.76	<u>92.78</u>
PM-5	I	<u>99.99</u>	<u>99.99</u>	<u>99.99</u>	<u>99.99</u>	99.99
	II	99.99	99.99	99.99	99.96	99.99
	III	99.99	99.99	99.99	99.99	<u>96.33</u>
PLS7-SB	I	<u>99.99</u>	<u>99.83</u>	<u>99.01</u>	99.64	<u>99.21</u>
	II	99.99	99.98	99.77	99.62	99.44
	III	99.99	99.99	99.91	<u>99.31</u>	99.54
PLS7-6Fold	I	<u>99.99</u>	<u>99.98</u>	<u>99.83</u>	99.91	<u>99.77</u>
	II	99.99	99.98	99.91	<u>99.78</u>	99.90
	III	99.99	99.99	99.99	99.94	99.77

5. Stiffness optimality for the worst multi-loadings

5.1. *Optimization to identify the worst loadings*

The above study investigated stiffness optimality of the considered PMs subjected to random multi-loadings, and thus might not catch the worst cases. Next, we proceed to identify the worst case multi-loadings that obtain the highest stiffness deficiency (or lowest stiffness optimality) for each PM. This can be numerically realized by solving the optimization problem

$$\begin{aligned} &\underset{\sigma_{pq}^{(r)}}{\text{Minimize}} \quad R = \frac{J_{\text{Rank6}}^{\text{opt}} \times \rho_{\text{Rank6}}}{J_{\text{PM}}^{\text{opt}} \times \rho_{\text{PM}}} \\ &\text{Subject to} \quad \|\mathbf{\Gamma}\|_{\text{F}}^2 \geq 0.01 \\ &\qquad\qquad -1 \leq \sigma_{pq}^{(r)} \leq 1, \quad (pq = 11, 22, 33, 23, 13, 12; r = 1, 2, ..., N_\sigma) \end{aligned} \tag{13}$$

where N_σ is manually specified by $2 \leq N_\sigma \leq 6$. The constraint on norm of $\mathbf{\Gamma}$ is imposed to prevent the stress terms becoming too small, which might cause numerical issues for optimization convergence. Again, the problem is solved in the low volume fraction limit.

Optimization problem (13) is solved in an embedded manner. In the inner processes, a multi-loading starting guess is provided, and the optimization problems in section 4 are solved to generate

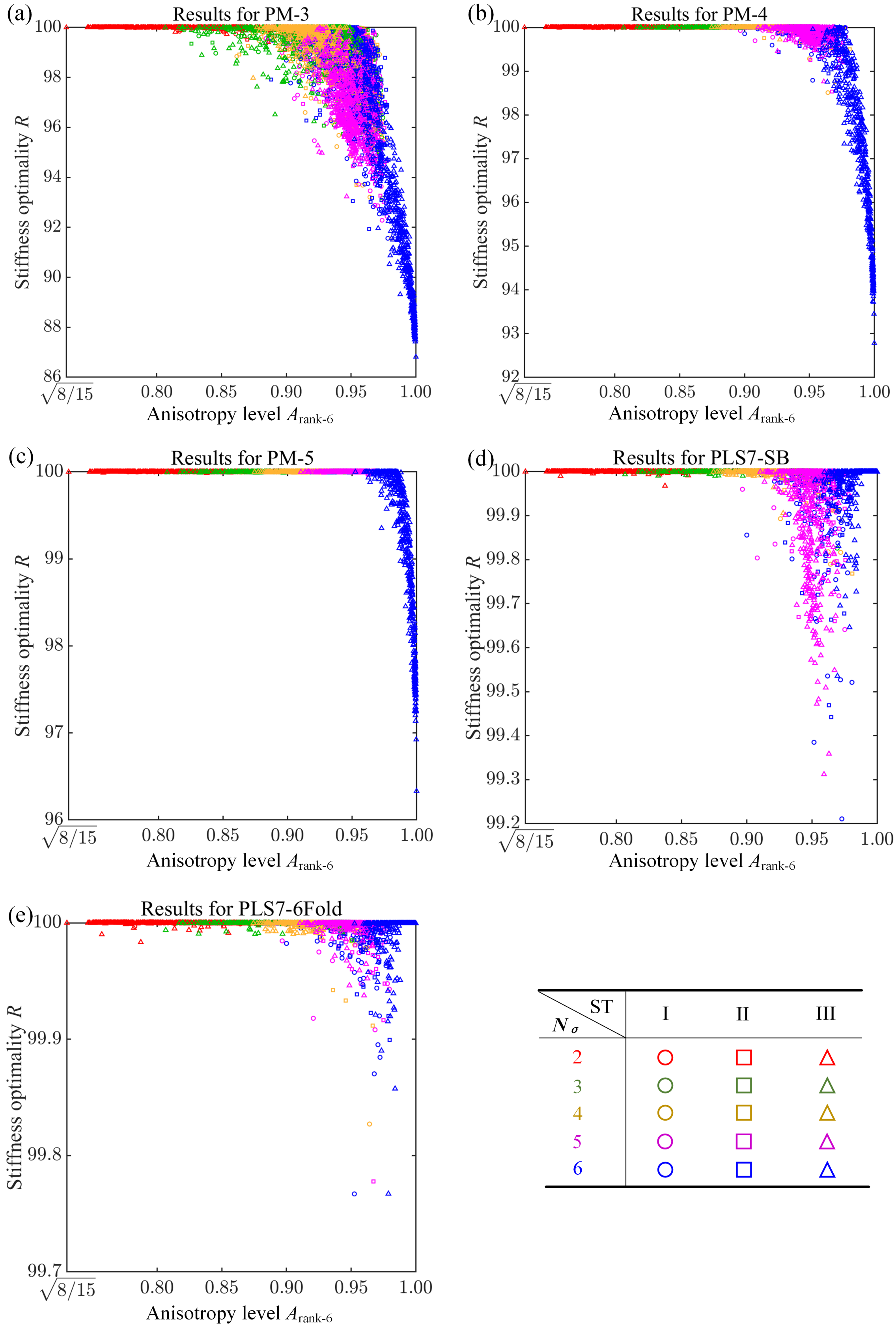

Figure 2: Energy ratios R with respect to anisotropy level of optimal rank-6 microstructures $A_{\mathrm{rank}-6}$ for various PMs. Different colors are used for various N_σ and different shapes are used for three stress generation strategies.

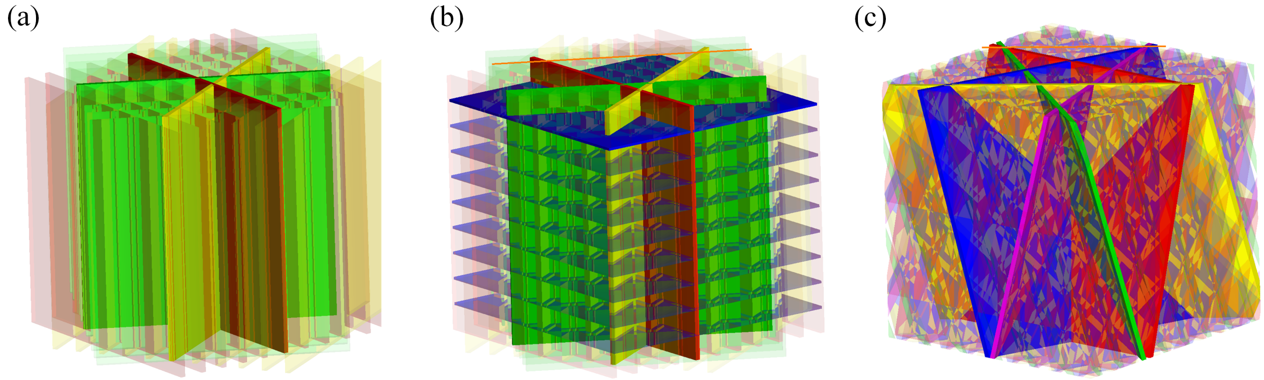

Figure 3: Optimized geometries by (a) PM-3, (b) PM-4 and (c) PM-5 in representative volume elements when subjected to isotropic multi-loadings. Various colors denote different plate sets. Solid plates are emphasized to illustrate the geometries and transparent plates indicate that infinite number of plates make up each plate set.

the extreme stiffness by the rank-6 microstructures as well as the maximum stiffness of each considered PM. In the outer process, optimization updates stress terms to find the worst multi-loading based on the result from the inner processes. In order to incorporate gradient-based optimizers, the derivative of the objective function is stated in terms of the derivative of the optimal stress energies with respect to each stress term, which reads

$$\frac{\partial J^{\mathrm{opt}}}{\partial \sigma_{pq}^{(r)}} = 2w_r (C_{pqmn}^{\mathrm{H}})^{\mathrm{opt}} \sigma_{mn}^{(r)} \tag{14}$$

In the implementation, all parameter settings for the inner optimizations are the same as section 4.3. In the outer process, the optimization is terminated if the relative difference of R values in two subsequent steps, as well as the constraint violence are smaller than 10^{-6}. For each PM at each N_σ, over 50 initial designs are applied, and the worst multi-loading is referred to the solution that has the smallest R^{opt} among all the optimized solutions. Note that only those initial guesses that generate non-extreme stiffness with $R < 1$ make sense in the optimizations, otherwise the procedure is terminated at the beginning. To fulfill this requirement, we partly select a number of multi-loadings that generated the optimized results with lowest R^{opt} in section 4.4 as the initial designs, and partly generate random initial stress cases that can obtain non-extreme stiffness via strategy I. If one PM achieves the extreme stiffness for over 10 thousand random initial guesses for a N_σ, it is accepted to be the optimal for any multi-loadings with N_σ stress cases.

A rigid rotation of all the stress cases in an optimized multi-loading results in a simultaneous rotation of the optimized rank-6 microstructures and the optimized PMs in the inner processes, and therefore it retains the optimized energy ratio R. This non-uniqueness may cause convergence issues when solving Eq. (13), since the optimal stress terms can be arbitrary numbers and infinite optimized solutions can be found. To address this issue, we fix the first stress case by aligning its three principal stresses with three coordinate axis over the entire optimization process. That is, three shear terms in the first stress case are set to be zero and they are excluded from the design variables. Consequently, we have $6N_\sigma - 3$ design variables in Eq. (13).

Based on the optimized results, we identify the worst multi-loadings as the eigentensors of $\mathbf{\Gamma}$

through

$$J = \Gamma_{ijkl} C^{\mathrm{H}}_{ijkl} = \sum_{r=1}^{N_\sigma} \tilde{w}^{(r)} \tilde{\sigma}^{(r)}_{ij} C^{\mathrm{H}}_{ijkl} \tilde{\sigma}^{(r)}_{kl} = \sum_{r=1}^{N_\sigma} \overline{\sigma}^{(r)}_{ij} C^{\mathrm{H}}_{ijkl} \overline{\sigma}^{(r)}_{kl} \tag{15}$$

subject to

$$\Gamma_{ijkl} \tilde{\sigma}^{(r)}_{ij} = \tilde{w}^{(r)} \tilde{\sigma}^{(r)}_{kl} \quad \text{and} \quad \overline{\sigma}^{(r)}_{ij} = \sqrt{\tilde{w}^{(r)}} \tilde{\sigma}^{(r)}_{ij} \tag{16}$$

where $\tilde{w}$ and $\tilde{\sigma}_{ij}$ indicate the eigenvalue and eigentensor of Γ, and the identified multi-loadings are formed by $\overline{\sigma}^{(r)}_{ij}$. In this way, each two stress cases of $\overline{\sigma}^{(r)}_{ij}$ are both linear independent and orthogonal. Note that only N_σ of the six eigenvalues are non-zero, and thus N_σ stress cases are reserved.

5.2. Results

The obtained worst multi-loadings for each PM at each N_σ are presented in Appendix A, and the corresponding energy ratios are given in Table 2 and are marked as hollowed samples in Fig. 4. Compared to the results in Table 1, the current results obtain higher stiffness deficiency with lower R values. This illustrates that the worst multi-loadings are difficult to be produced by using the random stress generation strategies as used in section 4. Moreover, these results show a monotonous degradation of stiffness optimality for the PMs as N_σ increases.

For $N_\sigma = 2$, PM-3 can still preserve over 95% of the extreme stiffness, but for $N_\sigma \geq 3$, its stiffness optimality drops to $R \approx 86\%$. By calculating the principal stresses of each stress case, it is found that the worst multi-loadings include near-pure shear stresses[1] in the second to final stress cases for $N_\sigma = 2, 3, ..., 6$. The orientations and magnitudes of these shear stresses vary with N_σ. The main reason for obtaining such kind of worst multi-loadings is that PM-3 has relatively low stiffness for shear loadings and therefore including more shear stresses leads to higher stiffness deficiency. For $N_\sigma = 6$, the final stress case has small values compared to the first five stress cases. As a consequence, it yields almost the same R value as the case of $N_\sigma = 5$. The worst multi-loadings for $N_\sigma = 5$ and 6 obtain a slightly higher stiffness deficiency than the result for the isotropic multi-loading. The optimized PM involves two plates with an equal $\tilde{t}$ and they are almost perpendicular to the third one.

PM-4 and PM-5 improve the stiffness optimality by including more plate sets. Therein, PM-4 attains the extreme stiffness for any $N_\sigma = 2$ multi-loadings, and obtains $R > 92\%$ for $N_\sigma \geq 3$. PM-5 attains the extreme stiffness for any multi-loadings with $N_\sigma \leq 4$, and obtains $R > 96\%$ for $N_\sigma \geq 5$. Their worst multi-loadings are not easily explained based on the numerical results, since the solutions include combinations of normal and shear stresses. The corresponding geometries are similar to the results for the isotropic multi-loading in section 4. For $N_\sigma = 5$ and 6, the optimized PM-4 is a full regular triangular prism with $\tilde{t}_{\mathrm{side}}/\tilde{t}_{\mathrm{base}} \approx 0.64$, and the optimized PM-5 has 5-fold symmetry, where the relative angle between each two neighboring plate sets becomes approximately 66-degree. In summary, PM-4 and PM-5 are good candidates to obtain any extreme stiffness for $N_\sigma = 2$ and $N_\sigma \leq 4$, respectively, and PM-6 has to be used for $N_\sigma \geq 5$.

The two PLS7s exhibit near-optimal stiffness in the worst multi-loadings for any N_σ. Here, PLS7-SB and PLS7-6Fold attain over $R > 97\%$ and $R > 99\%$ of the extreme stiffness for arbitrary multi-loadings. Slight stiffness deficiency for these two PLS7s is mainly caused by the implicit

[1]The principal stresses of a pure shear stress includes one zero and two opposite entries. Besides, if the summation of three principal stresses is zero, the stress behaves as a combination of multiple shear stresses, leading to isochoric deformations.

restrictions from geometric periodicity. The worst multi-loadings are combinations of normal and shear stresses. For $N_\sigma \geq 4$, the optimized PLS7-SB and PLS7-6Fold involve 6 and 5 plate sets with non-zero $\tilde{t}$, respectively. Note that although these results for the worst multi-loadings include fewer than 7 plate sets, the optimized PMs including all the 7 plate sets are necessary for other multi-loadings. In order to further increase stiffness optimality, one could use the PLSs that are formed by more plate sets, like the one which involves 3 simple, 4 body-centered and 6 face-centered plate sets [27]. However, this configuration might increase geometric complexity of the optimized PLSs.

In another testing, we apply the worst multi-loading of one PM on the others and evaluate the maximum stiffness by solving Eq. (2). The results are presented in Fig. 4. It is observed that each PM gains larger R values when subjected to the worst multi-loadings for other PMs than the case subjected to its own worst multi-loading. This illustrates that the worst multi-loadings are different for various PMs. Hence, if the applied multi-loading is the worst multi-loading for one PM, another PM can be used for higher stiffness.

Table 2 Energy ratios of considered PMs at their worst multi-loading.

N_σ	2	3	4	5	6
PM-3	95.15	87.12	86.85	86.19	86.15
PM-4	99.99	94.20	94.20	92.15	92.15
PM-5	99.99	99.99	99.99	96.23	96.22
PLS7-SB	99.99	99.34	97.85	97.83	97.83
PLS7-6Fold	99.99	99.65	99.45	99.45	99.45

We further compare stiffness optimality of these PMs under various Poisson's ratios of the solid constituents. The Poisson's ratios vary within the interval of $-0.99 \leq \nu_0 \leq 0.49$, where the maximum and minimum values are close to admissible upper and lower bounds for isotropic block materials. In each testing, the worst multi-loading and the corresponding stiffness optimality is obtained based on 50 solutions. The results are presented in Fig. 5. It is observed that the highest stiffness deficiency of these PMs is dependent on ν_0. In general, they have the best stiffness optimality for $\nu_0 = -0.99$, and their stiffness optimality decays as ν_0 increases. At each ν_0, PM-4 and PM-5 attain the extreme stiffness for any $N_\sigma = 2$ and $N_\sigma \leq 4$ multi-loadings, respectively. At $\nu_0 = 0.49$, the PLS7-SB and PLS7-6Fold suffer from the worst stiffness optimality for $N_\sigma = 5$ and 6, but they can still obtain $R > 97\%$ and $R > 99\%$ of the extreme stiffness, respectively.

6. Conclusion

We have investigated stiffness optimality of several PMs subjected to various types of multi-loadings. Based on the numerical results with respect to both random and the worst multi-loadings, we conclude that in the low volume fraction limit, PM-3, PM-4 and PM-5 can attain over 83%, 90% and 95% of the extreme stiffness for arbitrary multi-loadings, respectively. This stiffness optimality may be good enough for most practical applications if considering their simple geometries with fewer than 6 plate sets. Moreover, simple periodicity of PM-3 and PM-4 might have benefits in practical manufacturing. Furthermore, we identify two optimal PLSs, which are formed by 7 plate sets with defined connections, which achieve near-optimal stiffness for any multi-loadings. These PMs provide

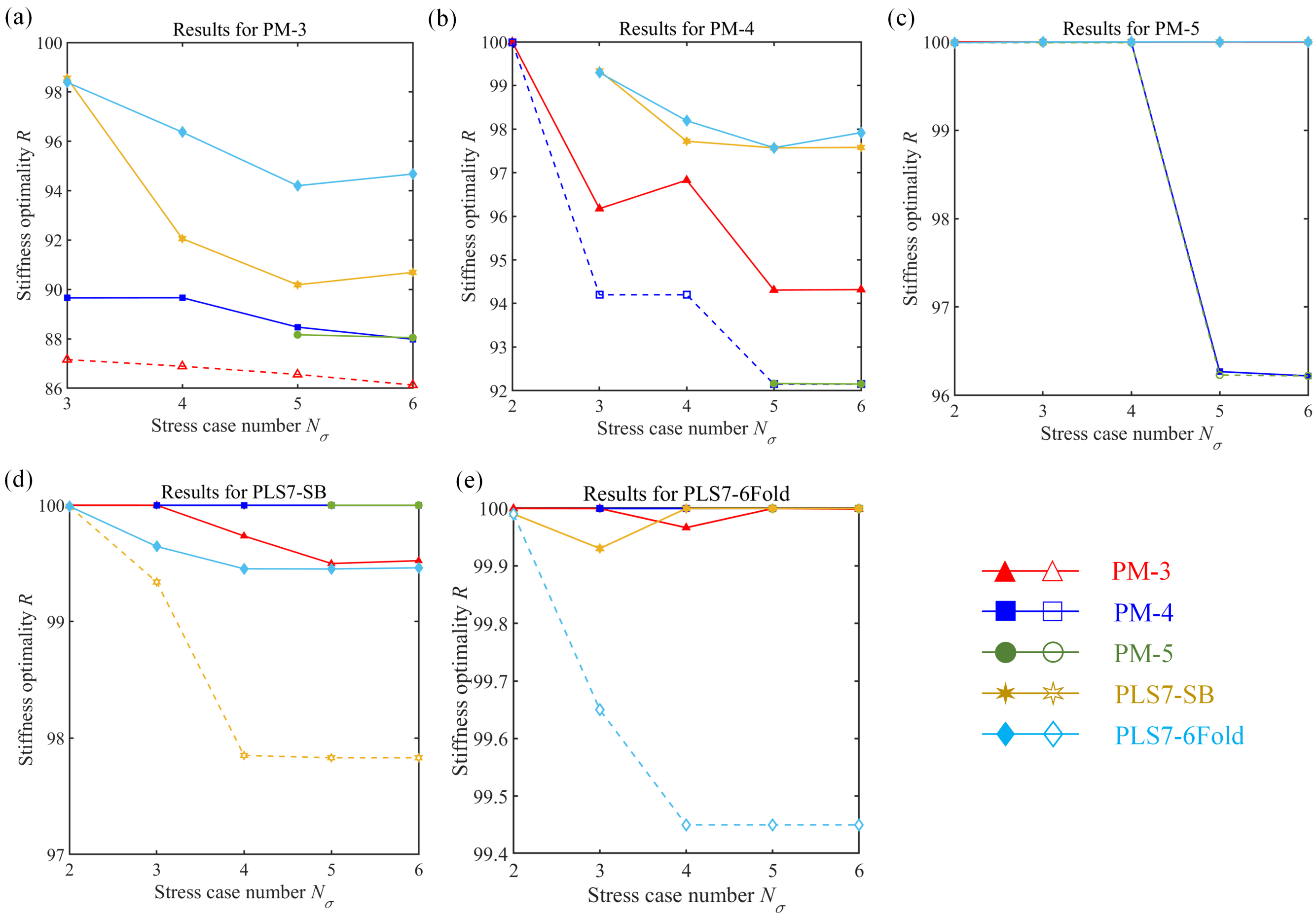

Figure 4: Stiffness optimality of PMs subjected to the worst multi-loadings for other PMs. Dashed lines with hollow samples indicate stiffness optimality of one PM subjected to its own worst multi-loading, and solid lines with filled samples denote stiffness optimality of one PM subjected to the worst multi-loadings for other PMs. Different colored samples indicate the worst multi-loadings for different PMs.

good candidates for achieving optimal stiffness for any specific multi-loadings, and using them in a multi-scale structural design framework may generate optimal structures with ultimate stiffness [10, 46, 47].

Besides stiffness, it is also crucial to investigate strength of the optimal PMs and to make a critical comparison with the truss microstructures. In the low volume fractions, the PMs involve thin plate members and thus they mainly suffer from buckling failure. Our recent study [48] has shown that although the PMs have higher stiffness than the truss microstructures, they have lower buckling strength. As the volume fraction increases, yield failure becomes dominating. It is of importance to identify the volume fractions for the transition between the two failure modes for the PMs. This future work would be fundamental to design advanced anisotropic mechanical metamaterials with both high stiffness and superior strength in a systematic manner [48]. Fabrication of these closed-walled PMs is quite challenging. By using 3D printing, one way is to make holes in the plates to remove enclosed fluid, powders or support materials [27, 49, 50].

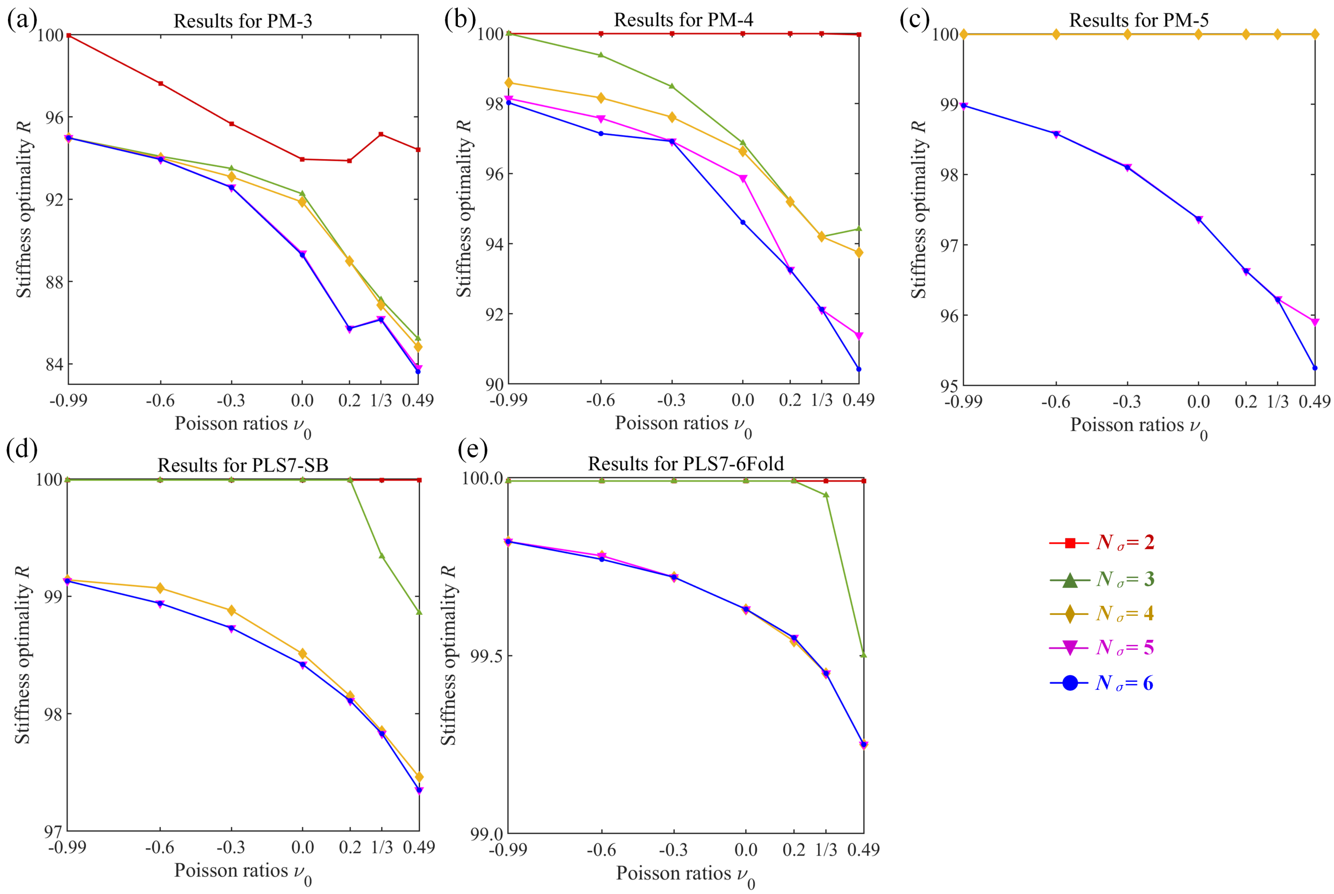

Figure 5: Stiffness optimality dependence on ν_0 for the considered PMs. Different colored samples denote the results for various N_σ.

Acknowledgment

Support from the Fundamental Research Funds for the Central Universities (DUT19RC(3)072) for Y. Wang and from the Villum Investigator Project InnoTop for J.P. Groen and O. Sigmund.

References

[1] M. Kadic, G. W. Milton, M. v. Hecke, W. Martin, 3d metamaterials, Nature Reviews Physics 1 (2019) pp.198–210.

[2] J. U. Surjadi, L. Gao, H. Du, X. Li, X. Xiong, N. X. Fang, Y. Lu, Mechanical metamaterials and their engineering applications, Advanced Engineering Materials 21 (2019) 1800864.

[3] X. Yu, J. Zhou, H. Liang, Z. Jiang, L. Wu, Mechanical metamaterials associated with stiffness, rigidity and compressibility: A brief review, Progress in Materials Science 94 (2018) pp.114–173.

[4] X. Zheng, H. Lee, T. H. Weisgraber, et al., Ultralight, ultrastiff mechanical metamaterials, Science, 344 (2014) pp.1373–1377.

[5] L. R. Meza, A. J. Zelhofer, N. Clarke, A. J. Mateos, D. M. Kochmann, J. R. Greer, Resilient 3d hierarchical architected metamaterials, Proceedings of the National Academy of Sciences 112 (37) (2015) 11502–11507.

[6] L. R. Meza, S. Das, J. R. Greer, Strong, lightweight, and recoverable three-dimensional ceramic nanolattices, Science 345 (2014) pp.1322–1326.

[7] G. W. Milton, A. V. Cherkaev, Which elasticity tensors are realizable?, J. Eng. Mater. Technol., 117 (1995) pp.483–493.
[8] M. Kadic, T. Bückmann, N. Stenger, M. Thiel, M. Wegener, On the practicability of pentamode mechanical metamaterials, Applied Physics Letters 100 (19) (2012) 191901.
[9] T. Bückmann, M. Thiel, M. Kadic, R. Schittny, M. Wegener, An elasto-mechanical unfeelability cloak made of pentamode metamaterials, Nature Communications 5 (2014) 4130.
[10] J. P. Groen, O. Sigmund, Homogenization-based topology optimization for high-resolution manufacturable microstructures, Int. J. Numer. Methods Eng., 113 (2018) pp.1148–1163.
[11] Y. Wang, L. Zhang, S. Daynes, Z. Hongying, S. Feih, M. Y. Wang, Design of graded lattice structure with optimized mesostructures for additive manufacturing, Materials and Design 142 (2018) pp.114–123.
[12] M.-S. Pham, C. Liu, l. Todd, J. Lertthanasarn, Damage-tolerant architected, Nature 565 (2019) pp.305–311.
[13] T. Frenzel, M. Kadic, M. Wegener, Three-dimensional mechanical metamaterials with a twist, Science 358 (6366) (2017) 1072–1074.
[14] T. Bückmann, M. Kadic, R. Schittny, M. Wegener, Mechanical cloak design by direct lattice transformation, Proceedings of the National Academy of Sciences 112 (16) (2015) 4930–4934.
[15] Z. Gan, M. D. Turner, M. Gu, Biomimetic gyroid nanostructures exceeding their natural origins, Science Advances 2 (5) (2016) pp.e1600084.
[16] Y. Yang, X. Song, X. Li, Z. Chen, C. Zhou, Q. Zhou, Y. Chen, Recent progress in biomimetic additive manufacturing technology: From materials to functional structures, Advanced Materials 30 (36) (2018) 1706539.
[17] J. Bauer, L. R. Meza, T. A. Schaedler, R. Schwaiger, X. Zheng, L. Valdevit, Nanolattices: An emerging class of mechanical metamaterials, Advanced Materials 29 (40) (2017) pp.1701850.
[18] X. Zhang, A. Vyatskikh, H. Gao, J. R. Greer, X. Li, Lightweight, flaw-tolerant, and ultrastrong nanoarchitected carbon, Proceedings of the National Academy of Sciences 116 (14) (2019) 6665–6672.
[19] X. Zhang, Y. Wang, B. Ding, X. Li, Design, fabrication, and mechanics of 3d micro-/nanolattices, Small 16 (15) (2020) 1902842.
[20] Z. Hashin, The elastic moduli of heterogeneous materials, J. Appl. Mech., 29 (1962) pp.143–150.
[21] R. Christensen, Mechanics of low density materials, J. Mech. Phys. Solids, 34 (1986) pp.563–578.
[22] V. S. Deshpande, N. A. Fleck, M. F. Ashby, Effective properties of the octet-truss lattice material, J. Mech. Phys. Solids, 49 (2001) pp.1747–1769.
[23] S. Vigdergauz, Two-dimensional grained composites of extreme rigidity, J. Appl. Mech., 61 (1994) pp.390–394.
[24] O. Sigmund, On the optimality of bone microstructure, in: IUTAM Symposium on Synthesis in Bio Solid Mechanics,, Springer, 1999, pp. pp.221–234.
[25] O. Al-Ketan, R. Rezgui, R. Rowshan, H. Du, N. X. Fang, R. K. Abu Al-Rub, Microarchitected stretching-dominated mechanical metamaterials with minimal surface topologies, Advanced Engineering Materials 20 (9) (2018) 1800029.
[26] J. Berger, H. Wadley, R. McMeeking, Mechanical metamaterials at the theoretical limit of isotropic elastic stiffness, Nature, 543 (2017) pp.533–537.
[27] T. Tancogne-Dejean, M. Diamantopoulou, M. B. Gorji, C. Bonatti, D. Mohr, 3d plate-lattices: An emerging class of low-density metamaterial exhibiting optimal isotropic stiffness, Advanced Materials 30 (45) (2018) 1803334.
[28] M. C. Messner, Optimal lattice-structured materials, J. Mech. Phys. Solids, 96 (2016) pp.162–183.
[29] R. M. Latture, M. R. Begley, F. W. Zok, Design and mechanical properties of elastically isotropic trusses, J. Mater. Res., 33 (2018) pp.249–263.
[30] G. Gurtner, M. Durand, Stiffest elastic networks, Proceedings of the Royal Society A: Mathematical, Physical and Engineering Sciences, 470 (2014) pp.20130611.
[31] Y. Wang, O. Sigmund, Quasiperiodic mechanical metamaterials with extreme isotropic stiffness, Ex-

treme Mechanics Letters 34 (2020) 100596.
[32] S. Ole, N. Aage, E. Andreassen, On the (non-)optimality of michell structures, Structural and Multidisciplinary Optimization 54 (2016) pp.361–373.
[33] P. Pedersen, On optimal orientation of orthotropic materials, Structural optimization, 1 (1989) pp.101–106.
[34] G. A. Francfort, F. Murat, Homogenization and optimal bounds in linear elasticity, Arch. Ration. Mech. Anal., 94 (1986) pp.307–334.
[35] K. A. Lurie, A. V. Cherkaev, Exact estimates of the conductivity of a binary mixture of isotropic materials, Proceedings of the Royal Society of Edinburgh Section A: Mathematics, 104 (1986) pp.21–38.
[36] G. Milton, Modelling the properties of composites by laminates, in: Homogenization and effective moduli of materials and media, Springer, 1986, pp. pp.150–174.
[37] B. Bourdin, R. V. Kohn, Optimization of structural topology in the high-porosity regime, J. Mech. Phys. Solids, 56 (2008) pp.1043–1064.
[38] O. Sigmund, A new class of extremal composites, J. Mech. Phys. Solids, 48 (2000) pp.397–428.
[39] Y. Wang, J. P. Groen, O. Sigmund, Simple optimal lattice structures for arbitrary loadings, Extreme Mechanics Letters 29 (2019) 100447.
[40] J. P. Groen, F. C. Stutz, N. Aage, J. A. Bærentzen, O. Sigmund, De-homogenization of optimal multiscale 3d topologies, Computer Methods in Applied Mechanics and Engineering 364 (2020) 112979.
[41] G. Francfort, F. Murat, L. Tartar, Fourth-order moments of nonnegative measures on s2 and applications, Arch. Ration. Mech. Anal., 131 (1995) pp.305–333.
[42] G. Allaire, Shape optimization by the homogenization method, Springer Science & Business Media, 2002.
[43] A. Cherkaev, Variational methods for structural optimization, Vol. 140, Springer Science & Business Media, 2002.
[44] A. F. Bower, Applied mechanics of solids, CRC press, 2009.
[45] M. M. Mehrabadi, S. C. Cowin, Eigentensors of linear anisotropic elastic materials, The Quarterly Journal of Mechanics and Applied Mathematics 43 (1) (1990) 15–41.
[46] P. Geoffroy-Donders, G. Allaire, O. Pantz, 3-d topology optimization of modulated and oriented periodic microstructures by the homogenization method, Journal of Computational Physics 401 (2020) 108994.
[47] L. Xia, P. Breitkopf, Concurrent topology optimization design of material and structure within fe2 nonlinear multiscale analysis framework, Computer Methods in Applied Mechanics and Engineering 278 (2015) pp.524–542.
[48] M. Andersen, F. Wang, O. Sigmund, On the competition for ultimately stiff and strong architected materials, Submitted.
[49] C. Crook, J. Bauer, A. G. Izard, C. S. de Oliveira, J. M. d. S. e Silva, J. B. Berger, L. Valdevit, Plate-nanolattices at the theoretical limit of stiffness and strength, Nature communications 11 (1) (2020) 1–11.
[50] S. Duan, W. Wen, D. Fang, Additively-manufactured anisotropic and isotropic 3d plate-lattice materials for enhanced mechanical performance: Simulations & experiments, Acta Materialia 199 (2020) 397–412.

Appendix A. Worst multi-loadings for PMs

This appendix presents the worst multi-loadings for various PMs at each N_σ. For the case that a specific PM can achieve extreme stiffness for arbitrary multi-loadings, no worst multi-loadings are obtained.

Table A1 Worst multi-loadings for PM-3 at each N_σ

N_σ	2		3			4			
σ_{11}	-0.572	0.001	-0.040	-0.002	0.004	-0.999	-0.002	0.003	0.027
σ_{22}	0.112	-0.001	1.000	0.001	0.002	-0.955	-0.006	0.000	-0.028
σ_{33}	1.000	0.004	1.000	0.001	0.000	-0.004	-0.005	0.001	0.007
σ_{23}	0.000	0.004	0.000	-0.001	0.000	0.000	0.025	-0.539	0.004
σ_{13}	0.000	-0.107	0.000	-0.032	0.612	0.000	0.659	0.020	0.000
σ_{12}	0.000	0.328	0.000	0.613	0.032	0.000	0.001	-0.005	-0.379

N_σ	5					6					
σ_{11}	0.440	0.503	-0.005	-0.039	-0.006	0.458	-0.474	0.031	-0.015	-0.168	0.008
σ_{22}	0.530	-0.471	0.020	0.004	0.004	0.516	0.447	-0.076	0.023	0.163	0.008
σ_{33}	0.999	0.029	-0.009	0.014	0.001	0.999	-0.015	0.007	-0.004	-0.003	-0.008
σ_{23}	0.000	-0.036	0.007	-0.558	-0.015	0.000	0.013	-0.011	-0.551	0.016	0.000
σ_{13}	0.000	0.020	0.584	0.008	-0.028	0.000	0.069	0.565	-0.008	0.002	0.002
σ_{12}	0.000	0.005	0.033	-0.017	0.488	0.000	-0.166	0.017	0.013	0.465	0.000

Table A2 Worst multi-loadings for PM-4 at each N_σ

N_σ	3			4			
σ_{11}	-0.192	0.001	0.001	-0.191	0.013	-0.002	-0.023
σ_{22}	1.000	0.001	0.001	0.997	0.031	-0.002	0.036
σ_{33}	1.000	0.000	0.001	0.999	0.010	-0.007	-0.041
σ_{23}	0.000	0.000	0.000	0.000	-0.006	0.011	-0.087
σ_{13}	0.000	-0.640	0.004	0.000	-0.639	-0.027	0.005
σ_{12}	0.000	-0.004	-0.640	0.000	-0.025	0.638	0.002

N_σ	5					6					
σ_{11}	-0.957	-0.263	0.002	0.001	0.000	-0.949	-0.277	0.002	-0.002	0.000	-0.003
σ_{22}	0.252	0.968	-0.001	-0.011	0.004	0.234	0.972	0.009	0.016	-0.036	-0.003
σ_{33}	0.724	-0.684	0.003	0.000	-0.001	0.741	-0.662	0.002	-0.005	0.022	-0.003
σ_{23}	0.000	-0.002	-0.143	0.128	0.837	0.000	0.032	-0.119	-0.111	0.840	0.000
σ_{13}	0.000	0.003	0.855	0.017	0.141	0.000	-0.005	-0.821	0.268	-0.077	0.000
σ_{12}	0.000	-0.009	-0.005	-0.853	0.129	0.000	0.009	-0.255	-0.809	-0.142	0.000

Table A3 Worst multi-loadings for PM-5 at each N_σ

N_σ	5					6					
σ_{11}	-0.887	0.401	-0.019	-0.027	0.014	-0.854	0.491	0.031	-0.002	0.001	0.073
σ_{22}	0.057	-0.992	-0.048	0.107	0.015	-0.025	-0.997	-0.004	0.002	-0.005	0.069
σ_{33}	0.846	0.487	-0.020	-0.029	-0.026	0.875	0.451	0.029	0.000	0.000	0.073
σ_{23}	0.000	-0.064	0.268	-0.444	-0.658	0.000	-0.002	0.031	0.620	0.584	0.000
σ_{13}	0.000	0.039	0.786	0.363	0.052	0.000	-0.038	0.863	-0.030	-0.014	-0.005
σ_{12}	0.000	-0.064	0.267	-0.614	0.509	0.000	-0.004	-0.011	-0.595	0.610	0.000

Table A4 Worst multi-loadings for PLS7-SB at each N_σ

N_σ	3			4			
σ_{11}	-0.992	-0.083	0.116	-0.967	-0.251	0.044	-0.022
σ_{22}	0.131	-0.141	0.103	0.003	-0.724	0.072	0.001
σ_{33}	0.824	-0.050	0.127	0.966	-0.251	0.033	0.011
σ_{23}	0.000	0.216	-0.123	0.000	0.061	0.518	-0.298
σ_{13}	0.000	0.184	-0.010	0.000	-0.365	0.058	0.000
σ_{12}	0.000	0.425	0.137	0.000	0.065	0.517	0.302

N_σ	5					6					
σ_{11}	-0.871	-0.001	0.472	0.133	0.026	-0.856	-0.068	0.498	-0.089	0.056	0.000
σ_{22}	-0.008	-0.021	0.196	-0.463	-0.008	-0.011	0.001	0.153	0.466	-0.004	0.003
σ_{33}	0.867	0.020	0.480	0.120	0.014	0.858	0.001	0.498	-0.096	0.075	0.000
σ_{23}	0.000	0.611	-0.033	-0.031	0.298	0.000	-0.628	0.056	0.039	-0.275	0.000
σ_{13}	0.000	0.012	-0.125	0.239	0.002	0.000	-0.031	-0.100	-0.235	-0.006	0.006
σ_{12}	0.000	-0.613	-0.015	0.018	0.297	0.000	0.605	0.136	-0.022	-0.283	0.000

Table A5 Worst multi-loadings for PLS7-6Fold at each N_σ

N_σ	3			4			
σ_{11}	-0.991	0.114	-0.034	-0.895	-0.447	0.002	-0.013
σ_{22}	-0.192	0.105	-0.027	-0.090	0.203	-0.008	0.005
σ_{33}	0.990	0.138	-0.034	0.724	-0.527	0.027	-0.021
σ_{23}	0.000	0.458	-0.076	0.000	-0.024	-0.410	0.249
σ_{13}	0.000	0.086	0.097	0.000	0.033	0.025	0.013
σ_{12}	0.000	-0.185	-0.206	0.000	0.004	-0.356	-0.288

N_σ	5					6					
σ_{11}	-0.214	-0.015	-0.025	0.006	0.027	-0.978	0.094	-0.183	0.042	-0.005	0.000
σ_{22}	0.721	0.611	-0.020	-0.004	0.006	-0.108	0.160	0.356	-0.179	-0.030	0.002
σ_{33}	0.783	-0.561	-0.001	-0.019	0.002	0.355	0.490	-0.436	0.099	-0.014	0.001
σ_{23}	0.000	0.404	-0.015	0.013	-0.004	0.000	0.511	0.126	0.052	0.024	-0.002
σ_{13}	0.000	0.033	0.257	-0.373	0.000	0.000	-0.018	0.097	0.238	0.020	0.003
σ_{12}	0.000	0.016	-0.507	-0.187	-0.002	0.000	0.040	-0.225	-0.293	0.028	0.002